

1 **The benefit of brightness temperature assimilation for the SMAP**
2 **Level-4 surface and root-zone soil moisture analysis over**
3 **mainland China**

4 Jianxiu Qiu^{1,2}, Jianzhi Dong³, Wade T. Crow³, Xiaohu Zhang^{4,5}, Rolf H. Reichle⁶, Gabrielle J.
5 M. De Lannoy⁷

6 ¹Guangdong Provincial Key Laboratory of Urbanization and Geo-simulation, School of Geography and Planning, Sun
7 Yat-sen University, Guangzhou, 510275, China

8 ²Southern Laboratory of Ocean Science and Engineering (Guangdong, Zhuhai), Zhuhai, 519000, China

9 ³USDA ARS Hydrology and Remote Sensing Laboratory, Beltsville, MD 20705, USA

10 ⁴National Engineering and Technology Center for Information Agriculture, Nanjing Agricultural University, Nanjing,
11 China

12 ⁵Jiangsu Key Laboratory for Information Agriculture, Nanjing Agricultural University, Nanjing, China

13 ⁶Global Modeling and Assimilation Office, NASA Goddard Space Flight Center, Greenbelt, MD, USA

14 ⁷Department of Earth and Environmental Sciences, KU Leuven, Heverlee, Belgium

15 *Correspondence to:* Jianxiu Qiu (qiujianxiu@mail.sysu.edu.cn)

16 **Abstract.** The Soil Moisture Active Passive (SMAP) Level-4 (L4) product provides global estimates of surface soil
17 moisture (SSM) and root-zone soil moisture (RZSM) via the assimilation of SMAP brightness temperature (Tb)
18 observations into the Catchment Land Surface Model (CLSM). Here, using in-situ measurements from 2474 sites in
19 mainland China, we evaluate the performance of soil moisture estimates from the L4 data assimilation (DA) system
20 and from a baseline “open-loop” (OL) simulation of CLSM without Tb assimilation. Using random forest regression,
21 the efficiency of the L4 DA system (i.e., the performance improvement in DA relative to OL) is attributed to eight
22 control factors related to the CLSM and as well as tau-omega radiative transfer model (RTM) components of the L4
23 system. Results show that the Spearman rank correlation (R) for L4 SSM with in-situ measurements increases for 77%
24 of the in-situ measurement locations (relative to that of OL), with an average R increase of approximately 14% ($\Delta R =$
25 0.056). RZSM skill is improved for about 74% of the in-situ measurement locations, but the average R increase for
26 RZSM is only 7% ($\Delta R = 0.034$). Results further show that the SSM DA skill improvement is most strongly related to
27 the difference between the RTM-simulated Tb and the SMAP Tb observation, followed by the error in precipitation
28 forcing [data](#) and [estimated](#) microwave soil roughness [parameter](#) h . For the RZSM DA skill improvement, these three
29 dominant control factors remain the same, although the importance of soil roughness exceeds that of the Tb simulation
30 error, as the soil roughness strongly affects the ingestion of DA increments and further propagation to the subsurface.
31 For the skill of the L4 and OL estimates themselves, the top two control factors are the precipitation error and the
32 SSM-RZSM coupling strength error, both of which are related to the CLSM component of the L4 system. Finally, we
33 find that the L4 system can effectively filter out errors in precipitation. Therefore, future development of the L4 system
34 should focus on improving the characterization of the SSM-RZSM coupling strength.

35

36 **Keywords.** SMAP Level 4, soil moisture, data assimilation, attribute analysis, random forest regression

37 **1 Introduction**

38 Soil moisture modulates water and energy feedback between the land surface and the lower atmosphere by determining
39 the partitioning of incoming net radiation into latent and sensible heat (Seneviratne et al., 2010, 2013). High-quality,
40 global-scale soil moisture products have become increasingly available in recent years. In particular, the L-band NASA
41 Soil Moisture Active Passive (SMAP) satellite mission (Entekhabi et al., 2010; Piepmeier et al., 2017) has significantly
42 improved the skill of available, global-scale soil moisture products. However, the SMAP observations contain temporal
43 data gaps and are only representative of conditions within only the first 5 cm of the vertical soil moisture column
44 (Entekhabi et al., 2010). To address these limitations, the SMAP Level-4 Surface and Root-Zone Soil Moisture (L4)
45 algorithm assimilates SMAP brightness temperature (Tb) observations into the NASA Catchment Land Surface Model
46 (CLSM) to derive an analysis of surface (0–5 cm) and root-zone (0–100 cm) soil moisture estimates with global, 3-
47 hourly coverage (Reichle et al., 2017a; Reichle et al., 2017b; Reichle et al., 2019).

48 However, the performance of a land data assimilation (DA) system is sensitive to the DA parameterization and requires
49 careful assessment. For instance, Reichle et al. (2008) demonstrate that DA based on incorrect assumptions of modeling
50 errors and observation errors can degrade soil moisture estimates, compared with the case of not performing DA, which
51 is commonly referred to as the “open-loop” (OL) baseline. Theoretically, the optimality of DA can be evaluated using

52 so-called “innovations”, or observation-minus-forecast residuals; however, an investigation of the innovations alone
53 is often insufficient to determine if the soil moisture analysis is optimal, as the innovations are affected by multiple
54 factors (Crow and Van Loon, 2006).

55 Recently, Dong et al. (2019a) proposed a novel statistical framework for evaluating the performance of a soil moisture
56 DA system. Specifically, they demonstrated that the relative skill of surface soil moisture (SSM) estimates acquired
57 with and without DA can be estimated using the ratio of their correlations with just one noisy but independent ancillary
58 remote sensing product. This approach was applied to the SMAP L4 system using Advanced Scatterometer soil
59 moisture retrievals. Their results show that the benefit of SMAP DA is closely related to densities of both rain gauge
60 and vegetation. Generally, higher rain gauge density indicates lower error in precipitation forcing, and lower vegetation
61 density indicates higher background model performance - both conditions lead to reduced SMAP DA benefit. However,
62 due to the limited availability of independent root-zone soil moisture (RZSM) products for performing statistical error
63 estimation, this method is only applicable for SSM estimates.

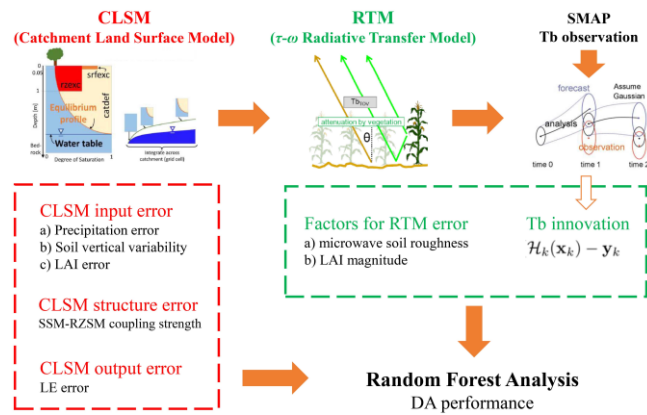
64 Relative to SSM, the efficiency of assimilating land surface observations to improve RZSM is complicated by model
65 structural error that affects the ability of the DA to update unobserved model states. For instance, Kumar et al. (2009)
66 identified the surface–root zone coupling strength, which is the result of a model-dependent representation of processes
67 related to the partitioning of rainfall into infiltration, runoff, and evaporation components, as an important factor for
68 determining RZSM improvement associated with the assimilation of SSM retrievals. Their synthetic experiments
69 suggest that, faced with unknown true subsurface physics, overestimating the surface–root zone coupling in the land

70 model is a more robust strategy for obtaining skill improvements in the root zone than under-estimating the coupling.
71 Likewise, Chen et al. (2011) suggested that the Soil and Water Assessment Tool significantly under-predicts the
72 magnitude of vertical soil water coupling in the Cobb Creek Watershed in southwestern Oklahoma, USA, and this lack
73 of coupling impedes the ability of DA to effectively update soil moisture in deep layers, groundwater flow and surface
74 runoff. In the context of the present paper, the evaluation of L4 RZSM estimates has been limited to SMAP core
75 validation and sparse network sites (Reichle et al., 2017a; Reichle et al., 2017b; Reichle et al., 2019). With such limited
76 validation sites, the RZSM skill of the L4 product at the global scale remains uncertain.

77 The primary objective of this study is to assess the DA skill improvement of the L4 product, i.e., the performance
78 improvement in L4 DA results relative to the OL baseline ~~of the L4 product~~, and to further determine how DA skill
79 improvement varies as a function of the major aspects in the system. As mentioned above, the modeling portion of the
80 L4 system consists of two components: land surface modelling (LSM) and radiative transfer modelling (RTM).
81 Therefore, we select control factors from each of the two components. For the LSM component, the errors can be
82 attributed to potential factors including: 1) model input forcing errors of a) precipitation, ~~and~~ b) leaf area index (LAI)
83 and c) the presence of vertical variability in soil properties; 2) model structure errors in ~~a)~~ characterizing SSM-RZSM
84 coupling strength ~~and b) the presence of vertical variability in soil properties~~; 3) model output error of LE. For the
85 RTM component, errors are characterized by: 1) ~~DA-Tb innovation~~, i.e., SMAP-observed minus RTM-simulated Tb;
86 2) the environmental factors that complicate the DA analysis when assimilating Tb observations, which include the
87 magnitude of a) microwave soil roughness and b) LAI. Figure 1 illustrates the conceptual relationship between these

Commented [JQ1]: Thank you for pointing this out. Throughout the manuscript, all mentioning of "Tb error" is modified to "Tb innovation".

88 factors. Specifically, precipitation and LAI are selected since they have been proven important for SMAP L4 SSM
 89 accuracy in a previous study (Dong et al., 2019a). The presence of errors in the vertical variability of soil properties
 90 and SSM-RZSM coupling strength are selected because both factors control the propagation of soil moisture error
 91 from the surface soil layer to deeper layers, and we focus on both the SSM and RZSM retrieval accuracy. Error in
 92 CLSM LE output is selected because of its connection between the water and energy balance. Error in Tb innovation
 93 is selected because of its direct impact on the size of the DA update. Error in microwave soil roughness is selected
 94 owing to its high sensitivity to RTM accuracy. These eight control factors from the above-mentioned five aspects
 95 determine the crucial aspects of both the LSM and RTM components in the L4 system and are readily quantifiable
 96 using remote sensing products. Thus, they are selected to investigate the mechanism underlying the L4 improvement
 97 observed in this study.



98

99 **Figure 1: Systematic connection in the DA framework, and the association between the eight selected factors in the**

100

analysis.

101

102 Therefore, to achieve the two major objectives, we first evaluate the performance of L4 SSM and RZSM estimates
103 using 2474 sites in mainland China with soil moisture profile measurements (generally acquired at sub-surface depths
104 between 10 and 50 cm) during the two-year period of 2017 to 2018. Next, the in-situ measurements are used to assess
105 the DA skill improvement of the L4 system, which is defined as the skill difference between the L4 estimates and the
106 OL baseline. Additionally, we apply a machine-learning technique to quantify by how much the eight potential control
107 factors drive the spatial variations in the efficiency of the L4 system. In this way, we seek to prioritize future
108 enhancements to the L4 system.

109 **2 Data and Methods**

110 In this section, we briefly describe the SMAP L4 soil moisture product (Section 2.1), the network of in-situ soil
111 moisture observations in mainland China (Section 2.2), the above-mentioned control factors and ancillary data sources
112 (Section 2.3), and the vertical coupling metric used in the skill assessment (Section 2.4). Next, we introduce the double
113 instrumental variable (IVd) method employed to determine the errors in control factors that cannot be determined using
114 ground observations (Section 2.5). Finally, we describe the random forest (RF) regression method used to identify the
115 main factor(s) (out of the eight control factors from both CLSM and RTM aspects) that affect the spatial variations in
116 SMAP L4 DA skill improvement and L4 performance (Section 2.6).

117 **2.1 SMAP L4 soil moisture product**

118 The SMAP L4 soil moisture product (version 4; Reichle et al., 2019) is generated by assimilating the SMAP L1C
119 Radiometer half-orbit 36 km Equal-Area Scalable Earth (EASE) Grid Tb observations (Version 4 SPL1CTB; Chan et
120 al., 2016) into the CLSM. The SMAP Tb observations are assimilated at 3-h intervals using a spatially distributed, 24-
121 member ensemble Kalman filter (Reichle et al. 2017b). The surface meteorological forcing data are from the global
122 Goddard Earth Observing System (GEOS) Forward Processing atmospheric analysis (Lucchesi, 2013), with
123 precipitation corrected using the daily, 0.5-degree, gauge-based Climate Prediction Center Unified (CPCU) product
124 (Xie et al. 2007). The L4 product provides global, 9-km, 3-hourly surface (0–5 cm) and root-zone (0–100 cm) soil
125 moisture estimates along with related land surface fields and analysis diagnostics. For the present study, we aggregate
126 all soil moisture estimates to daily averaged (00:00 to 23:59 UTC) data. The OL baseline is a model-only, ensemble
127 CLSM simulation without the assimilation of SMAP Tb observations but otherwise using the same configuration,
128 including perturbations, as in the L4 system (Reichle et al., ~~2020~~2021).

129 The SMAP L4 assimilation system includes a zero-order “tau-omega” forward RTM (De Lannoy et al., 2013) that
130 converts SSM and surface soil temperature into L-band brightness temperature estimates. Select parameters of the L4
131 RTM, including the: microwave soil roughness parameter h , vegetation structure parameter τ , and the microwave
132 scattering albedo ω , are calibrated using multi-angular L-band brightness temperature observations from the Soil
133 Moisture Ocean Salinity (SMOS) mission (De Lannoy et al., 2014a). The L4 RTM parameterizes microwave soil
134 roughness as a function of SSM (De Lannoy et al., 2013, their equation B1). Here, we use this parameterization to

Commented [JQ2]: Many thanks to the Reviewer #1 for the meticulous comment!
In this case, the equation we quoted here is actually from Appendix B of the citation, namely De Lannoy et al. (2013), which should be the equation B1 of P782.

135 compute the 2017-2018 daily averaged microwave soil roughness estimates as one potential indicator of DA skill
136 improvement (Section 2.3). The necessary parameters are obtained from L4 “Land-Model-Constants” output
137 Collection (last access: 8 July 2020; DOI: <https://doi.org/10.5067/KGLC3UH4TMAQ>; Reichle et al., 2018a). The L4
138 “Analysis-Update-Data” output Collection includes RTM predictions of Tb and the assimilated SMAP Tb observations
139 (last access: 8 July 2020; DOI: <https://doi.org/10.5067/60HB8VIP2T8W>; Reichle et al., 2018b).

140 To avoid the impact of seasonality, we perform our analysis using anomaly time series, derived by subtracting a
141 seasonally varying (daily) climatology from each raw time series. The climatology of a given time series is obtained
142 by sampling the mean value of all soil moisture estimates that fall within a 31-day moving window centered on a
143 particular day-of-year. Moreover, L4 estimates of land latent heat flux (LE), land sensible heat flux (SH) and the
144 climatological LAI inputs to CLSM and the RTM, are obtained from the L4 “Geophysical-Data” output Collection
145 (last access: 6 April 2020; DOI: <https://doi.org/10.5067/KPJNN2GIIDQR>; Reichle et al., 2018c). These datasets are
146 also used to compute control factors to explain spatial variations in the DA skill improvement of the L4 system (Section
147 2.3).

148 **2.2 Soil moisture validation data**

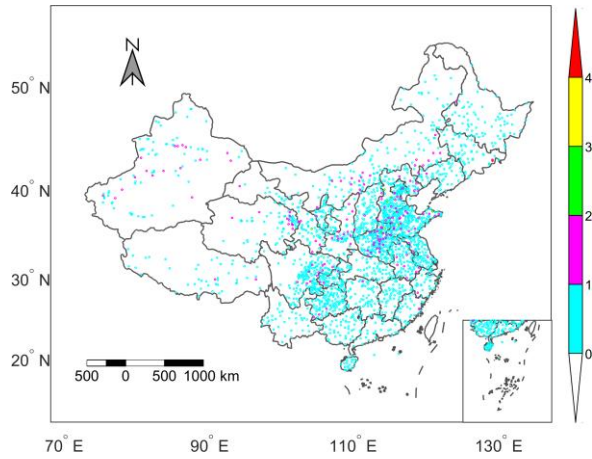
149 In-situ soil moisture measurements during 2017 and 2018 are collected from a national network of Chinese Automatic
150 Soil Moisture Observation Stations (CASMOs) maintained by the Chinese Meteorological Administration (CMA;
151 Han et al., 2017). In total, soil moisture measurements from 2474 separate stations array across mainland China, and
152 covering different land use types, are collected. At each CASMOs site, frequency domain reflectometry-based

153 instruments (DNZ1, DNZ2, and DNZ3) are used to record hourly volumetric soil moisture content within the following
154 vertical depth ranges: 0–10, 10–20, 20–30, 30–40, and 40–50 cm below the surface. This instrumentation – DNZ1,
155 DNZ2 and DNZ3 – is separately produced by Shanghai Changwang Meteorological Science and Technology
156 Corporation (Shanghai, China), Henan Meteorological Science Research Institute and the 27th Institute of China
157 National Electric Power Corporation (Zhengzhou, China), and China Huayun Technology Development Corporation
158 (Beijing, China), respectively. From the above-mentioned instruments, the These hourly estimates (at multiple depths)
159 are then aggregated into daily values and linearly averaged (vertically) to produce 0-10 cm (SSM) and 0-50 cm (RZSM)
160 in situ soil moisture measurements – which are subsequently used to validate the L4 and OL SSM (0-5 cm) and RZSM
161 (0-100 cm) estimates. Note that Spearman correlation rather than Pearson correlation is used for L4 and OL validation
162 because Pearson correlation assumes linear consistency of the underlying variables and is more sensitive to outliers.
163 By employing Spearman’s rank correlation, we ~~avoid introducing ad-hoc thresholds and~~ do not need to exclude soil
164 moisture outliers ~~and thus avoid introducing ad-hoc thresholds that would define outliers~~. Nonetheless, we repeat the
165 analysis based on Pearson correlation (not shown) and find that the results are qualitatively consistent with the results
166 using Spearman’s correlation.
167 Ground observations within the same 9-km EASE grid were averaged for comparisons against the collocated 9-km L4
168 and OL soil moisture estimates. A total of 2287 individual 9-km EASE grid cells within mainland China are included
169 in the analysis. Among them, 92.35% of grid cells contain one in-situ site, 7.26% contain two sites, 7 grid cells contain

Commented [RRH(63)]: Many thanks to the suggestions from Reviewer #1 to add the definition of soil moisture outlier. Our understanding is that we do NOT exclude outliers in the computation of Spearman correlation, so we do not need to provide a precise definition of outliers. We do not present the results of Pearson correlation, which might have required us to exclude outliers. But since we don't use Pearson correlation, there's no need to be specific. We hope the revised text would clear this point up.

Commented [CW4R3]: Agreed

170 three sites, and the remaining two grid cells contain four and five sites respectively. Figure 42 shows the number of
171 in-situ CASMOS sites within each 9-km EASE grid.



172

173 **Figure 42:** The number of in-situ CASMOS sites within each 9-km EASE grid across mainland China.
174

175 2.3 Explanatory data products

176 As discussed above, our hypothesis is that the efficiency of the SMAP L4 system will be sensitive to the ability of the
177 ensemble-based L4 analysis in filtering errors that exist in CLSM, the RTM forecast Tb, and the assimilated SMAP
178 Tb observations. We therefore consider two separate categories of factors that potentially control spatial variations in
179 DA skill improvement. The factors are summarized in Table 1.

180 The first category represents a range of factors known to affect the skill of soil moisture estimates derived from the
181 LSM (in this case, CLSM). The five control factors in this category are: 1) the error in precipitation forcing, 2) the
182 error in (input) LAI, 3) the error in (output) LE, 4) the magnitude of mean error in CLSM SSM-RZSM coupling
183 strength, and 5) the presence of vertical variability in soil properties (defined as the difference in clay fraction across
184 the vertical soil profile). Note that such variability represents a potential source of error because, with the exception of
185 some surface-layer moisture transport parameters, CLSM assumes soil texture and associated soil parameters are
186 vertically homogeneous within the soil column. However, the Harmonized World Soil Database (HWSD;
187 [FAO/IIASA/ISRIC/ISSCAS/JRC, 2012](#)) often captures distinct vertical variations in soil properties, ~~which, therefore,~~
188 ~~since it is largely~~ neglected by CLSM. ~~Therefore,~~ the magnitude of vertical heterogeneity in soil texture may be an
189 effective proxy for overall CLSM soil moisture accuracy. [HWSD is selected due to its extensive use in soil science](#)
190 [\(De Lannoy et al., 2014b\), and switching from HWSD to the high-resolution soil hydraulic and thermal properties](#)
191 [dataset derived from Global Soil Dataset for Earth System Models and SoilGrids \(Dai et al., 2019\) does not](#)
192 [qualitatively change our conclusion, or the importance ranking of vertical variability in soil properties \(figure not](#)
193 [shown\).](#) In addition, [given the high specific surface area of clay and its high influence on soil structure and aggregation,](#)
194 [the clay fraction is very important for soil moisture retention \(Hillel, 1998\), and thus clay fraction is chosen over silt](#)
195 [and sand fractions in the analysis. Besides,](#) note that since LH and SH are generally (strongly) anti-correlated, it is not
196 appropriate to include both in a single random forest analysis – since including both would yield biased (high)
197 regression weights for LH and SH.

198 The second category contains three factors that affect radiative transfer modeling (RTM) and therefore DA updates.

199 These include: 1) estimates of the ~~DA-Tb~~ innovation, namely difference between SMAP Tb observations and RTM
200 Tb simulations, 2) the magnitude of microwave soil roughness, and 3) the magnitude of LAI (as a proxy for the
201 vegetation optical depth at microwave frequencies, which modulates the contribution of surface soil to the observed
202 Tb).

203 The control factors take a variety of forms. Some factors are based on estimates of the errors fed into the L4 system,
204 namely: 1) the error in CLSM rainfall forcing data; 2) error in SSM-RZSM coupling strength; 3) vertical variability of
205 clay fraction; 4) SMAP L4 LAI error; 5) output LE error; 6) ~~Tb~~-error in Tb innovation. Other factors consist of the
206 magnitude of the variable itself, namely the magnitude of microwave soil roughness and annual mean LAI. Note that
207 LAI is used in both ways: LAI error is used to predict OL performance (because LAI is an important input into CLSM),
208 while mean LAI is used to explain DA performance (because increased LAI is associated with decreased soil moisture
209 information in microwave observations).

210 Note that the LAI used in the L4 system is a merged climatology from Moderate Resolution Imaging Spectroradiometer
211 (MODIS) and Geoland data based on satellite observations of the Normalized Difference Vegetation Index (Mahanama
212 et al., 2015; Reichle et al., 2017a). Therefore, to indicate the magnitude by which the LAI of each grid cell typically
213 deviates from its long-term climatology, we use the temporal standard deviation for the anomaly time series of a
214 benchmark LAI time series as a measure of the error in the LAI value used in the L4 system. This benchmark LAI is
215 from the SPOT-Vegetation (SPOT VGT) product and includes inter-annual variations (Section 2.3.3). Owing to the

216 lack of reference Tb observations at similar satellite overpass times and locations, ~~Tb~~-errors in Tb innovation are
217 gauged using the time series standard deviation of the observation-minus-forecast (O-F) Tb residuals, which indicate
218 the typical misfit between the model forecast Tb and the rescaled SMAP Tb observations. This rescaling process
219 ensures zero-mean differences between Tb observations and forecasts and involves a seasonal multiyear-mean bias
220 correction, which makes sure that the DA only corrects for errors in short-term and inter-annual variations and not for
221 errors in the climatological seasonal cycles of the modeled soil moisture or other land surface fields. The standard
222 deviation of the O-F Tb residuals measures the total error in Tb observation space.

223 The exact data sets and the metrics utilized for evaluating all eight control factors are summarized in Table 1.

Table 1 Benchmark data sets and metrics used for evaluating control factors of SMAP L4

Factor category	Control factor	Dataset/Benchmark	Temporal resolution	Spatial resolution	Data range	Metrics
LSM	Precipitation error	Rain gauge (CGDPA)	daily	0.25 °	2017-2018	Spearman's rank correlation R
	SSM-RZSM coupling strength error	CASMOS	daily	NA	2017-2018	ΔCP (see Section 2.4)
	Vertical variability of clay fraction	HWSO	NA	9 km	NA	Difference in clay fraction between topsoil (0-30 cm) and root-zone (0-100 cm) layers
	SMAP L4 LAI error	SPOT-VGT LAI	10 d	1 km	2017-2018	Temporal standard deviation of SPOT VGT LAI anomaly
	LE error	FLUXCOM	daily	(1/120) °	2017-2018	IVd-based R
RTM	Tb error <u>Error in Tb innovation</u>	SMAP L4	daily	9 km	2017-2018	Temporal standard deviation of O-F Tb residuals
	Microwave soil roughness	SMAP L4	daily	9 km	2017-2018	Temporal average based on De Lannoy et al. (2013)
	Annual mean LAI	MODIS/Geoland-based product	daily	9 km	2017-2018	Climatological mean

226 **2.3.1 Gauge-based precipitation gridded product**

227 Errors in the precipitation data used to force the CLSM within the SMAP L4 system are estimated via Spearman's
228 rank correlation with available rain-gauge observations. These network observations are based on an analysis of ~2400
229 rain gauge stations distributed across mainland China (Shen et al., 2015). Recently, the China Gauge-based Daily
230 Precipitation Analysis (CGDPA) with a spatial resolution of $0.25^{\circ} \times 0.25^{\circ}$ based on this network was constructed and
231 has been made operational over mainland China (last access: 28 April 2020;
232 http://data.cma.cn/data/cdcdetail/dataCode/SEVP_CLI_CHN_PRE_DAY_GRID_0.25.html). CGDPA uses a
233 modified version of climatology-based optimal interpolation (OI) with topographic correction proposed by Xie et al.
234 (2007). In this process, the daily precipitation climatology over mainland China is optimized and rebuilt using the 30-
235 year average precipitation observations from ~2400 gauges of the period 1971–2000 (Shen et al., 2010). CGDPA is
236 shown to have smaller bias and root mean square error (for instance, $13.51 \text{ mm day}^{-1}$ vs. $17.02 \text{ mm day}^{-1}$ for
237 precipitation of $25.0\text{--}50.0 \text{ mm day}^{-1}$) than the CPCU product used in the SMAP L4 system, which is based on fewer
238 than 400 gauge sites over mainland China (Shen et al., 2015).

239 **2.3.2 FLUXCOM LE estimates**

240 The FLUXCOM ensemble of global land-atmosphere energy fluxes is used to evaluate error in L4 LE estimates. This
241 ensemble merges energy flux measurements from FLUXNET eddy covariance towers with remote sensing and
242 meteorological data based on four broad categories of machine learning method (namely tree-based methods,
243 regression splines, neural networks, and kernel methods) to estimate global gridded net radiation, latent and sensible

244 heat and their related uncertainties (Jung et al., 2019). The resulting FLUXCOM database has a 0.0833 ° spatial
245 resolution when applied using MODIS remote sensing data. The monthly energy flux data of all ensemble members,
246 as well as the ensemble estimates from the FLUXCOM initiative, are freely available (CC4.0 BY license) from the
247 Data Portal (<http://fluxcom.org/>), while the daily- and 8-day FLUXCOM products are available upon request from
248 dataset provider Martin Jung (last access: 14 April 2020). To calculate the LE error, we collected the daily, high spatial
249 resolution FLUXCOM product and extracted the LE estimates where in-situ soil moisture sites are located.

250 **2.3.3 SPOT VGT LAI**

251 The data set used as a benchmark for assessing leaf area index (LAI) errors present in the SMAP L4 analysis is derived
252 from the SPOT/VEGETATION and PROBA-V LAI products (version 2) that generated every 10 days (at best) with a
253 spatial resolution of 1 km. The SPOT LAI version 2 product GEOV2 is provided by the Copernicus Global Land
254 Service (last access: 15 April 2020; <https://land.copernicus.eu/global/products/LAI>; Baret et al., 2013). It capitalizes
255 on the development of already existing products: CYCLOPES version 3.1 and MODIS collection 5 based on neural
256 networks (Baret et al., 2013; Verger et al., 2008). Compared to version 1, the version 2 products are derived from top
257 of canopy daily reflectances, which ensures reduced sensitivity to missing observations and avoids the need for a
258 bidirectional reflectance distribution function model.

259 **2.3.4 HWSD soil texture**

260 The soil texture information is from the HWSD attribute database (v1.2; FAO/ILASA/ISRIC/ISSCAS/JRC, 2012),
261 which is a 30 arc-second raster database with 15773 different soil-mapping units worldwide. It provides information
262 on the standardized soil parameters for topsoil (0–30cm) and subsoil (30-100 cm) separately. In this study, we use the
263 difference of clay fractions between topsoil (0-30cm) and the aggregated 0-100cm layer to measure the vertical clay
264 fraction variation at each 9-km grid cell.

265 **2.4 Vertical coupling metric**

266 The RZSM time series generally show decreased temporal dynamics relative to SSM. As a result, overestimated SSM-
267 RZSM coupling tends to spuriously increase the (correlation-based) similarity of SSM and RZSM time series, and
268 thereby, overestimate RZSM temporal variability. Therefore, analogous to Kling-Gupta efficiency (Gupta et al., 2009),
269 we define the SSM-RZSM coupling strength (CP) as:

$$CP = 1 - \sqrt{(R-1)^2 + (\alpha-1)^2} \quad (1)$$

270 where R is the Spearman's rank correlation between SSM and RZSM, and α is the ratio of temporal standard deviation
271 of SSM to that of RZSM. The CP estimation is based on anomaly time series of both SSM and RZSM. A CP value of
272 one represents the extreme case where RZSM is identical to SSM, i.e., a strongly coupled case. Likewise, a CP of zero
273 represents the opposing case of completely uncoupled time series. Cases with negative CP do not exist in this study.

274 Observed CP (CP_{obs}) was based on comparisons between 0-10 cm “surface” and 0-50 cm “root-zone” in-situ
275 observations and used as a benchmark. In contrast, CP estimates of OL (CP_{OL}) was based on the comparison of 0-5 cm
276 “surface” and 0-100 cm “root-zone” estimates. Therefore, the surface versus root-zone storage contrast in the
277 observation time series is less than that of the L4 estimates. This will likely cause the observed correlation between
278 surface and root-zone time series to be systematically higher than the analogous vertical correlation calculation for L4
279 estimates. However, this bias is partially corrected for by the second term in Eq. (1) – since the observed α ratio will,
280 by the same token, tend to be smaller (i.e. closer to one) than α sampled from the L4 analysis. Such ability to
281 compensate for vertical depth differences is a key reason we apply CP, rather than *simple correlation*, as a vertical
282 coupling strength metric. Nevertheless, it should be noted that our main interest here lies in describing spatial variations
283 in ($CP_{OL} - CP_{obs}$) and care should be taken when interpreting raw ($CP_{OL} - CP_{obs}$) differences as an *absolute* measure of
284 L4 vertical coupling bias.

285 **2.5 Double instrumental variable (IVd) method**

286 The benchmark data set of FLUXCOM LE described above contains error that is assumed to be of a similar order of
287 magnitude as the L4 LE dataset it is applied to evaluate. Therefore, in an attempt to correct for the impact of this error,
288 the LE error used here as a control factor is obtained via a double instrumental variable (IVd; Dong et al., 2019b)
289 analysis approach that minimizes the spurious impact of random errors in benchmark data sets. As shown in Dong et
290 al. (2019b), for the evaluation of two time series containing autocorrelated errors, IVd is more robust than a single
291 instrumental variable based algorithm, therefore we apply IVd to evaluate the LE error.

292 IVd is a modified version of triple collocation (TC) analysis. In TC analysis (McColl et al., 2014), geophysical
 293 variables obtained from three independent sources (x_t , y_t and z_t) at time t are assumed to be linearly related to the true
 294 signal P_t as:

$$x_t = \alpha_x P_t + B_x + \varepsilon_{x,t} \quad (2)$$

295 where the α_x is a scaling factor; B_x is a temporal constant bias and $\varepsilon_{x,t}$ is zero-mean random error.

296 As opposed to the TC method, IVd uses only two independent products (x , y) to characterize geophysical data product
 297 errors. This method introduces two instrumental variables I , which is the lag-1 time series of x , and J , which is the lag-
 298 1 time series of y , respectively.

$$I_t = \alpha_x P_{t-1} + B_x + \varepsilon_{x,t-1} \quad (3)$$

$$J_t = \alpha_y P_{t-1} + B_y + \varepsilon_{y,t-1} \quad (4)$$

299 Therefore, assuming that the errors of two independent products are serially white, the covariance between instrumental
 300 variables and products can be written as follows:

$$C_{Ix} = \alpha_x^2 L_{PP} \quad (5)$$

$$C_{Jy} = \alpha_y^2 L_{PP} \quad (6)$$

301 where C represents the covariance of the subscript products. For instance, C_{Ix} represents the covariance of x and its
302 instrumental variable I . Variable L_{pp} is the lag-1 auto-covariance of the true signal. Combining Eqs. (5) and (6), the
303 scaling ratio s_{ivd} of the two products x and y can be written as:

$$s_{ivd} = \sqrt{\frac{C_{Ix}}{C_{Iy}}} \quad (7)$$

304 Based on Eq. (7), their correlation with truth can be estimated as:

$$R_{Px}^2 = \frac{C_{xy}s_{ivd}}{C_{xx}} \quad (8)$$

$$R_{Py}^2 = \frac{C_{xy}}{C_{yy}s_{ivd}} \quad (9)$$

305 In this way, the error in the L4 LE (measured by IVd-based correlation with truth) can be estimated robustly using the
306 FLUXCOM LE product described in Section 2.3.2.

307 **2.6 Random forest regression**

308 A random forest (RF) regression approach is used to rank and quantify the importance of the eight control factors
309 introduced above (Table 1) for describing spatial patterns in DA skill improvement for both SSM and RZSM estimates.

310 The RF method is a supervised learning algorithm based on an averaged ensemble of decision trees (Breiman, 2001).

311 Unlike linear regression approaches, RF can capture non-linear interactions between the features and the target. In

312 addition, the normalization (or scaling) of data is not necessary in RF application. Another advantage of the RF

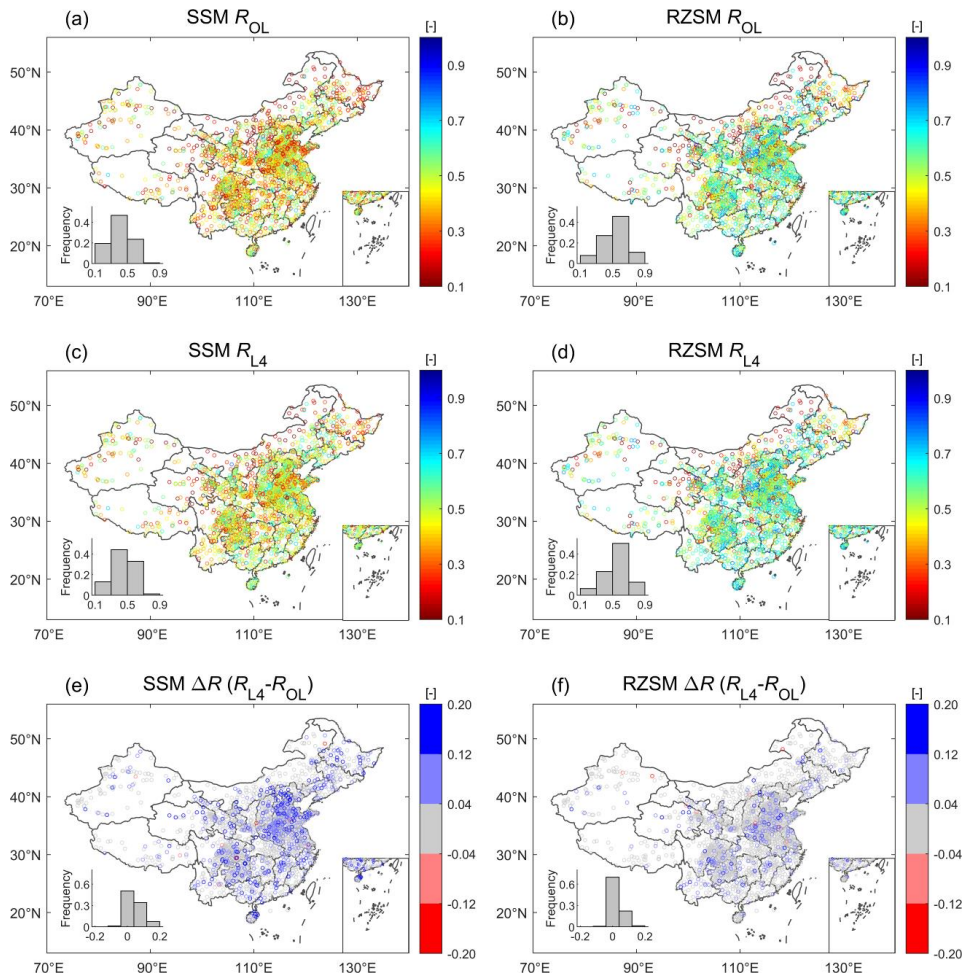
313 algorithm is that it can readily measure the relative importance of each feature on the estimates, which makes it highly
314 suitable for an attribution analysis. Therefore, based on the output of RF, key control factors determining the skill
315 improvement of SMAP DA are evaluated and ranked. The RF estimates are based on a 10-fold cross-validation
316 approach.

317 3 Results

318 3.1 Validation of SMAP L4 and OL estimates of SSM and RZSM anomalies

319 Figure 2-3 maps validation results (i.e., anomaly Spearman's rank correlation with in-situ observations, R) for SMAP
320 L4 and associated OL soil moisture estimates. The skill patterns for OL and L4 are, in general, quite spatially consistent.
321 Both are characterized by an increasing trend of SSM estimation skill moving from northwest to southeast China (Fig.
322 2a-3a and 2b3b) that matches the increasing density of the rain gauge network. In relative terms, the L4 product
323 surpasses the baseline OL's SSM skill for 77% of the 2287 9-km EASE grid cells containing ground observations –
324 with a mean R increase of $\Delta R = 0.056$ [-] and mean relative improvement versus R_{OL} of 14%.

325 Similar spatial patterns are observed for RZSM skill. As with SSM, generally higher consistency with in-situ RZSM
326 measurements is found in southeast China relative to northern and northwestern China. However, relative to SSM, the
327 benefit of SMAP data assimilation (i.e., L4) is reduced for RZSM and the mean relative R improvement is only 7%
328 ($\Delta R = 0.034$ [-]) (compare Fig. 2e-3e and 2f3f). This reduction is expected since assimilated SMAP Tbs are primarily
329 sensitive to soil moisture conditions in the surface (0-5 cm) layer.



330
 331 **Figure 23:** OL (a, b) and L4 (c, d) skills (R values) for SSM (left column) and RZSM (right column). DA skill improvement
 332 ($\Delta R = R_{L4} - R_{OL}$) for (e) SSM and (f) RZSM. Blue (red) colors in (e) and (f) indicate grid cells where L4 estimates are better
 333 (worse) than OL. Non-significant differences (based on a 1000-member bootstrapping analysis) are shaded grey. The lower
 334 left inset in each subplot indicates the frequency of binned R -values across all 9-km EASE grid cells containing ground
 335 observations.

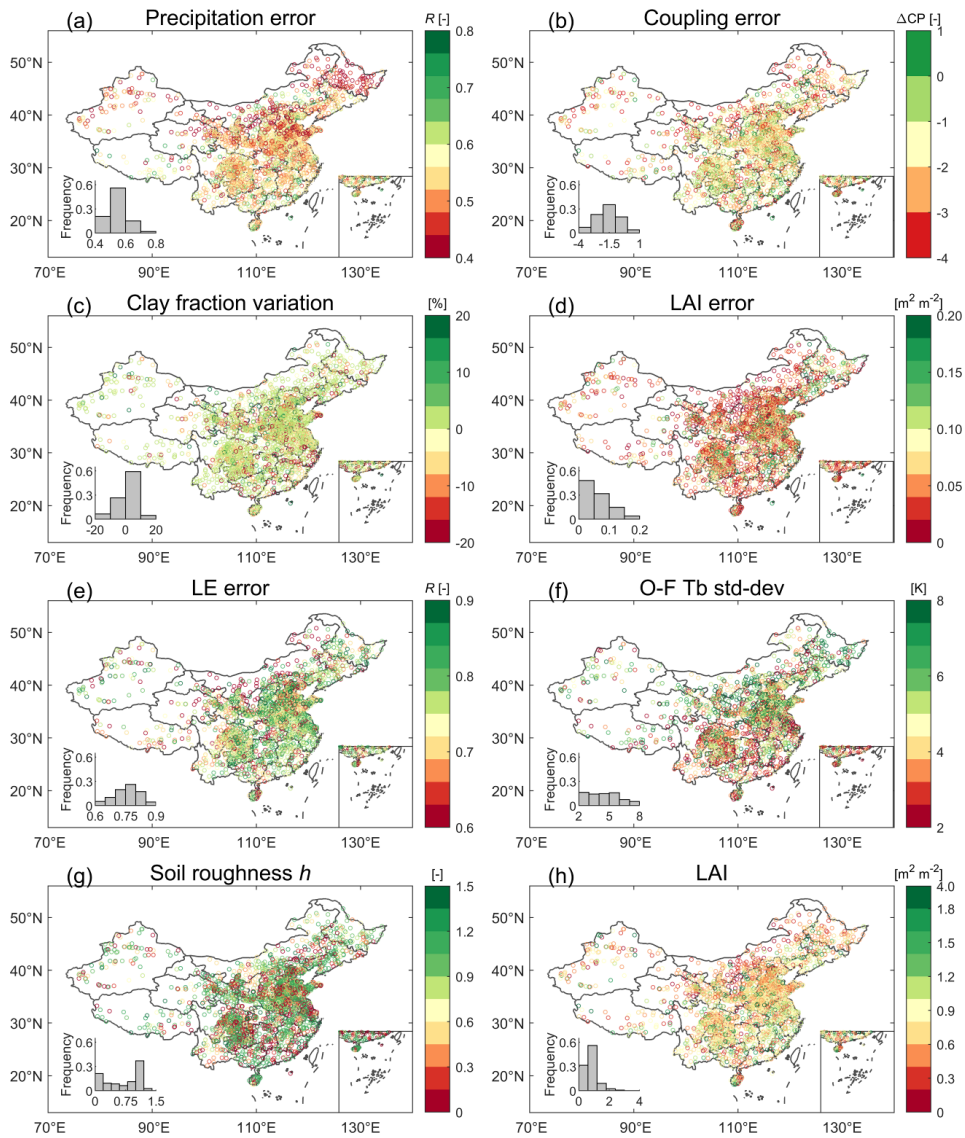
336

337 3.2 Spatial distribution of potential factors controlling SMAP L4 DA performance

338 As described in Section 2.3, we select eight control factors that potentially influence the skill of SMAP L4 soil moisture
339 estimates. Using the attribution analysis described in Section 2.6, these factors are used to explain the spatial variations
340 in skill and DA skill improvement seen in Fig. 23. As a first step, this section examines the spatial patterns inherent in
341 the eight control factors. Errors in the CLSM precipitation forcing are relatively higher in northern and northwestern
342 areas of China (Fig. 3a4a), where the gauge density is generally sparser than in southern China. Among the factors
343 representing CLSM structural errors, a pre-dominantly negative bias is observed in SSM-RZSM coupling strength
344 generally across China (i.e., lower CP_{OL} compared to CP_{obs}), while a very small number of grid cells show a positive
345 coupling strength bias in eastern China (dark green dots in Fig. 3b4b). This is expected since the coupling strength
346 generally decreases with coarser resolution, i.e., the vertical coupling strength of model is assumed much lower than
347 that of any single site. In addition, this may be partially attributed to layer depth differences, since CLSM represents
348 surface and root-zone depths of 0-5 cm and 0-100 cm, respectively, whereas the corresponding in-situ observations
349 represent the 0-10 cm and 0-50 cm layers. Therefore, CP_{OL} is likely to be systematically smaller than CP_{obs} . In addition,
350 the vertical variability of the clay fraction seems to show little spatial variation across mainland China (Fig. 3e4c).
351 With respect to CLSM LAI error, regions in southern China that have generally higher LAI show larger standard
352 deviations in SPOT LAI time series (Fig. 3d4d and 3b4h). The IVd-based estimates of SMAP L4 LE error, which

353 represent a potential control factor for water-balance errors in CLSM, generally show a low level of error across
354 mainland China (Fig. [3e4e](#)).

355 For O-F Tb residuals describing RTM-related error, a higher standard deviation of O-F Tb residuals is observed in the
356 North China Plain (Fig. [3f4f](#)), which is very consistent in spatial distribution with areas displaying the highest and
357 most significant SSM prediction improvement (Fig. [2e3c](#)). This is expected, as mentioned above, because O-F Tb
358 residuals are the basis for the soil moisture corrections (or increments) that are applied in the DA system as part of the
359 L4 analysis. The 2017-2018 mean of soil roughness shows a relatively scattered spatial pattern (Fig. [3g4g](#)), while the
360 2017-2018 mean LAI shows higher values in southwest and southeast China (Fig. [3h4h](#)).



361
 362 **Figure 34:** Factors potentially influencing SMAP L4 performance over mainland China: (a) CLSM precipitation error
 363 measured by the Spearman's rank correlation between CLSM precipitation and ground observations; (b) SSM-RZSM

364 coupling strength error (CP_{ol} minus CP_{obs}); (c) clay fraction variation (difference) across the soil profile; (d) error in LAI
365 input to L4; (e) IVD-based error of LE from L4; (f) O-F Tb standard deviation; (g) L4 microwave soil roughness; (h)
366 climatology mean of LAI input to L4. The last row shows factors that consist of the magnitude of the variable itself, while
367 the other rows show factors based on estimates of the errors that are fed into the L4 system.

368

369 3.3 Attribution of SMAP L4 versus OL performance to control factors

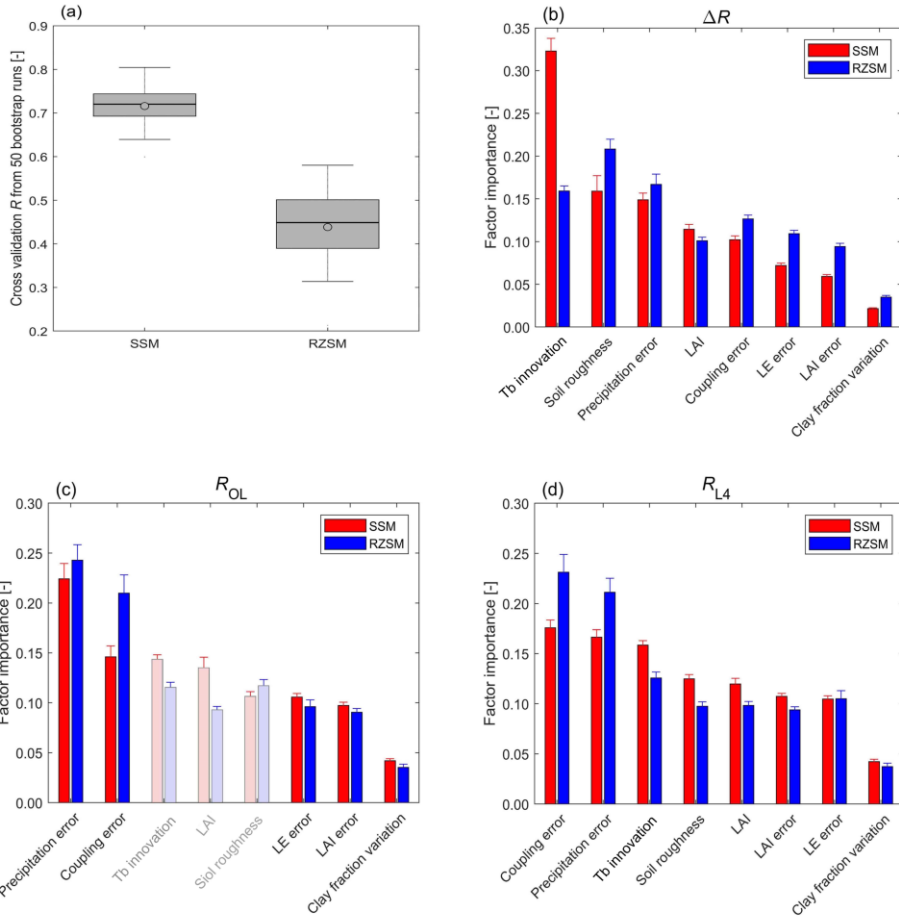
370 3.3.1 Attribution using random forest regression

371 As mentioned above, RF regression is used to identify the relative importance of our eight control factors for
372 determining the improvement of SMAP L4 DA (i.e., $\Delta R = R_{L4} - R_{OL}$) and also R_{L4} and R_{OL} . We first investigate the
373 robustness of RF for predicting ΔR . To estimate the magnitude of randomness in the RF algorithm, we use 50 bootstrap
374 runs. As shown in Fig. [4a5a](#), the 10-fold cross-validation test (228 validation samples) shows that the predicted and
375 in-situ-based ΔR have a mean correlation of 0.72 and 0.46 for SSM and RZSM, respectively. In Fig. [4a5a](#), the mean
376 and median of the cross-validation correlation are shown in black circle and black line respectively within the boxes,
377 while the second and third quartiles of the cross-validation correlation are shown as the edges of boxes.

378 Given the sampling errors of ΔR , which is based on a two-year validation period, and the relatively low spatial
379 variability in RZSM skill (Figs. 2f), the performance of RF is acceptable. In addition, ground-measurement upscaling
380 error is likely a significant contributor to unexplainable spatial variability for ΔR in Fig. [23](#). In fact, Chen et al. (2016)

381 found large spatial variability in the ability of point-scale SSM ground observations to describe grid cell-scale SSM
382 dynamics. In-situ observations sites associated with larger random point-to-grid upscaling errors will introduce a
383 spurious low bias into sampled estimates of ΔR values (see Appendix B in Dong et al., 2020). Therefore, part of the
384 ΔR spatial variability observed in Fig. 2-3 is unrelated to any aspect of the L4 system and, therefore, unexplainable via
385 our eight selected control factors.

386 Independent representativeness errors have an equal impact on both the L4 and OL skill assessments and should
387 therefore not bias the relative skill assessments of L4 versus OL, particularly when these assessments are based on
388 averaging across multiple grid cells. This holds if the location of ground-based measurements sites (within a footprint)
389 is purely random. For the systematic sampling errors, we analyze the site “representativeness” using the 500m MODIS
390 Land Cover product (MCD12Q1 v6) in 2017, IGBP dataset. First, we take the land cover (LC) type of the MODIS
391 grid cell where a given in-situ site is located as the ground-based LC type. Next, we search all the MODIS grid cells
392 that fall within the SMAP 9km EASE grid cell where this in-situ site is located. The latter area consists of about $20 \times$
393 $20 = 400$ MODIS grid cells. We calculate the fraction of these 400 MODIS grid cells that have the same LC type as
394 the ground-based LC and define this fraction as the site representativeness. We find that 52% of the 2474 sites have
395 site representativeness higher than 50%. When we use only these sites for the RF attribute analysis, the top three factors
396 controlling skill improvement ($R_{L4} - R_{OL}$), L4 skill (R_{L4}), and OL skill (R_{OL}) are still the same, although the
397 precipitation error becomes the top influencer for R_{L4} (not shown).



398

399 **Figure 45:** Attribution analysis of SMAP L4 DA skill improvement: (a) cross-validation of RF regression method in
 400 predicting DA skill improvement $\Delta R = R_{L4} - R_{OL}$ based on our eight control factors (Table 1). Relative importance of eight
 401 control factors determining spatial patterns in (b) DA skill improvement (ΔR), (c) OL performance (R_{OL}), and (d) L4
 402 performance (R_{L4}). Red (blue) bars represent predictor importance for SSM (RZSM). Error bars reflect the standard

403 deviation from 50-member bootstrapping of the RF importance estimates. [Since RTM-related errors do not impact the SM](#)
404 [skill in the OL simulation, the corresponding bars in panel \(c\) are shown as semi-transparent \(see text for details\).](#)

405
406 Based on the RF results, the Tb ~~innovation error~~ is quantified as the most prominent factor in determining DA skill
407 improvement (i.e., $\Delta R = R_{L4} - R_{OL}$) – followed by precipitation error and microwave soil roughness (Fig. [4b5b](#)). The
408 RF-derived ranking of control-factor importance for RZSM is similar to that of SSM in that the same three factors are
409 still the most explanatory. However, relative to SSM, the importance of Tb ~~innovation error~~ for RZSM decreased
410 dramatically from >30% to ~15%. Other modeling error sources (e.g., the vertical variability of soil properties) have
411 only very limited impacts on SMAP DA improvement.

412 As seen in Fig. [4e5c](#), for the OL performance (R_{OL}), the most important factors identified by RF include precipitation
413 error, SSM-RZSM coupling error, and Tb ~~innovation error~~ (microwave soil roughness) for SSM (RZSM). Note that
414 although the Tb ~~innovation error~~ is identified as [the](#) third-most important factor for R_{OL} in SSM skill, this is an instance
415 where correlation (i.e., poorer skill happens to coincide with higher Tb ~~innovation error~~) does not imply a causal
416 relationship. Specifically, it is expected that Tb ~~(Θ -F)innovations errors~~ are higher in areas where the OL performs
417 worse, but a high Tb ~~innovation error~~ is not the cause of a low OL performance. The same argument applies to the
418 relationship between microwave soil roughness and OL skill for RZSM estimation. To retain the consistency with [the](#)
419 analysis of R_{L4} and avoid the misconnection between RTM-related factors and R_{OL} , the bars representing the
420 importance of RTM-related factors to R_{OL} are set semi-transparent in Fig. [4e5c](#). The SMAP L4 system is able to reduce

421 impact of precipitation errors on both SSM and RZSM estimation skill, rendering SSM-RZSM coupling error the most
422 important factor for R_{L4} (Fig. 4e5d). In addition, in the L4 system, the high vegetation density effect on SSM and
423 RZSM estimation is clearly reduced, as the fourth-most important factor of LAI magnitude is replaced by Tb

424 ~~innovation error~~.

425 The qualitative rankings provided by the RF analysis in Fig. 4-5 are relatively robust to our particular choice of the
426 benchmark data set to define the ‘error’ of various control variables. For instance, we replace the CGDPA precipitation
427 benchmark with the Climate Prediction Center Morphing (CMORPH) merged product (Version 1, last access: 6 April
428 2020; DOI: <https://doi.org/10.25921/w9va-q159>; Xie et al., 2019), which is the 0.1 degree merging product of
429 CMORPH and observations from more than 30,000 automatic weather stations in mainland China. In this case, the
430 predictive power of the regression model established by the RF is not affected (similar to Fig. 4a5a), and the qualitative
431 rankings of the precipitation error in R_{OL} and R_{L4} are not impacted (similar to Fig. 4e5c-d).

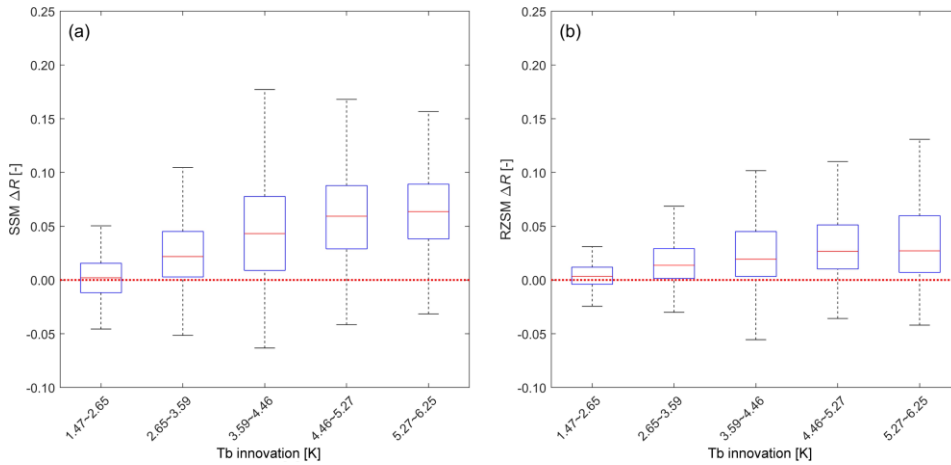
432

433 3.3.2 Attribution using box plot comparisons

434 As stated in Section 2.5, the RF method is adept at summarizing the impact of multiple (co-varying) control factors
435 simultaneously in the established regression model, and thus provides more comprehensive insights than the
436 examination of how the target variable (DA improvement) fluctuates with each individual control factor. However, it
437 does not allow the investigation of the sign of the relationship between DA improvement and each control factor –

438 which is important for understanding how each factor influences the DA system. In addition, since the net impact of
 439 various factors can enhance DA skill improvement by either degrading the OL or enhancing the ability of DA to add
 440 more value, it is important to decompose the source of variations in ΔR . Therefore, in addition to examining how
 441 SMAP DA skill improvement, i.e., $\Delta R = R_{L4} - R_{OL}$, varies as a function of the most prominent control factors identified
 442 above in Section 3.3.1 (i.e., Tb innovation error, precipitation forcing error, and microwave soil roughness). We also
 443 examine how precipitation error as a control factor affects the OL performance, i.e., R_{OL} .

444 To minimize the uncertainty caused by large errors in each of the control factors, we exclude samples with errors
 445 (separately for each control factor) ranking above the 80th percentile in the following analysis. The relationship
 446 between Tb innovations errors and L4 DA skill improvement is straightforward: higher Tb innovations errors are
 447 associated with higher ΔR , with ΔR generally larger for SSM than for RZSM (Fig. 5a6a-b).



448

449 **Figure 56:** SMAP L4 DA skill improvement ($\Delta R = R_{L4} - R_{OL}$) as a function of Tb innovation error for (a) SSM and (b) RZSM.

450 Samples with Tb innovation error ranking above the 80th percentile are excluded from the analysis.

451

452 For precipitation, this decomposition is illustrated in Fig. 67. Note that, as expected, low-quality precipitation tends to

453 degrade the skill (i.e., correlation versus ground observations) of OL SSM and RZSM estimates (see Fig. 6a7a-b). This

454 degradation provides an enhanced opportunity for SMAP L4 DA to provide benefit. As a result, ΔR tends to be a

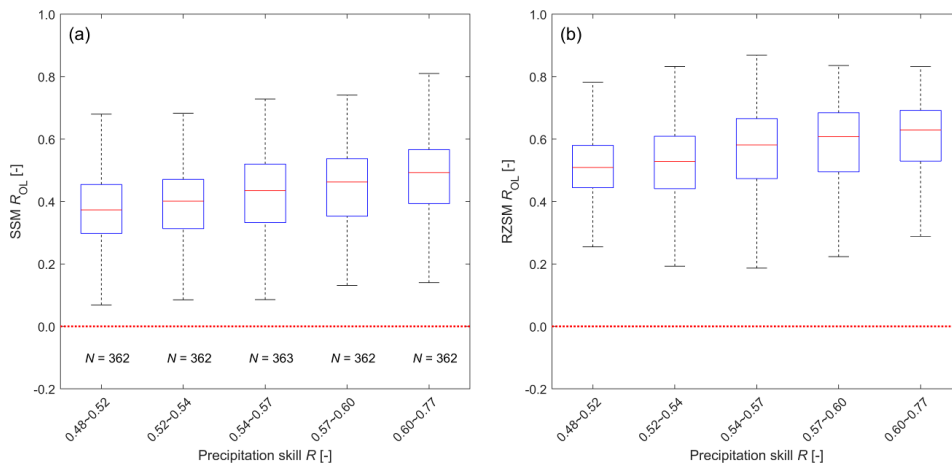
455 proportional function of precipitation skill (i.e., higher precipitation skill leads to lower ΔR , see Fig. 6e7c-d). This

456 inverse relationship is a well-known tendency for land data assimilation systems (Liu et al., 2011; Bolten and Crow,

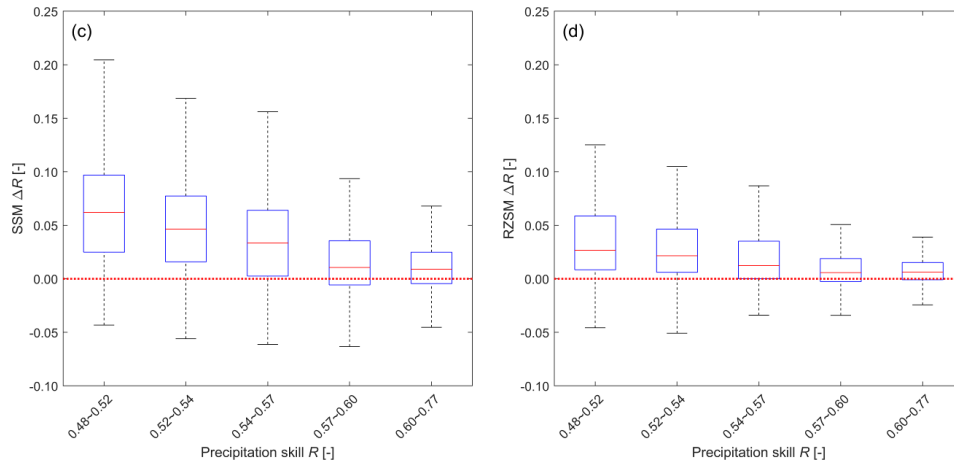
457 2012; Dong et al., 2019a). Precipitation quality has a diminished impact on RZSM estimation skill compared to SSM

458 estimation skill. This is expected since RZSM is (essentially) the result of applying a low-pass time series filter to

459 precipitation. As such, it is less sensitive to high-frequency errors in precipitation products than SSM is.



460

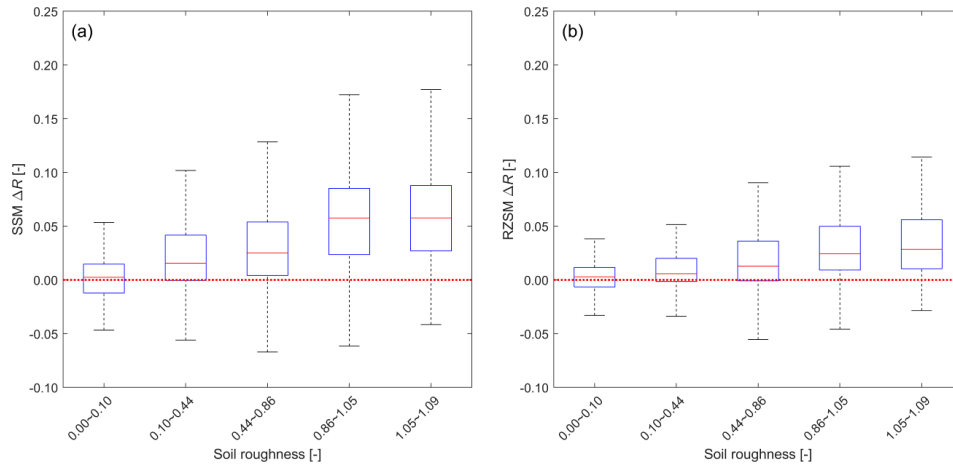


461

462 **Figure 7:** OL performance (R_{OL}) as a function of precipitation forcing skill R for (a) SSM and (b) RZSM. SMAP L4 DA
 463 skill improvement ($\Delta R = R_{L4} - R_{OL}$) as a function of precipitation skill for (c) SSM and (d) RZSM. Samples with precipitation
 464 skill ranking below the 20th percentile are excluded from the analysis.

465

466 Figure 7-8 is analogous to Fig. 5-6 but shows skill differences ΔR as a function of microwave soil roughness. Similar
 467 to Tb innovation errors, it is as expected that this control factor of microwave soil roughness has little impact on the
 468 OL performance, except that R_{OL} shows slight decreasing tendency with increasing soil roughness (not shown). Given
 469 the fact that the OL does get worse with increasing roughness, there is more room for improvement in areas with higher
 470 soil roughness, which makes it plausible that ΔR increases with increasing soil roughness (see Fig. 7a8a-b).



471

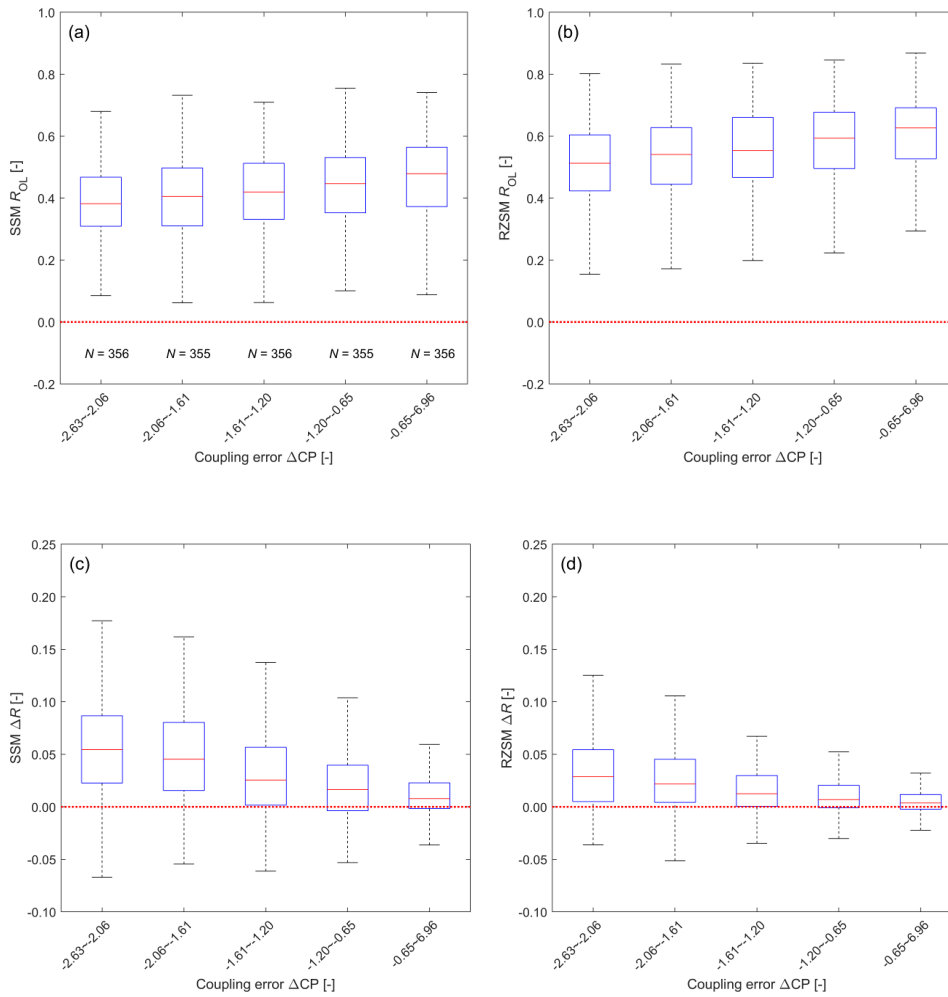
472 **Figure 78:** As in Fig. 5-6 but for ΔR as a function of microwave soil roughness.

473

474 Besides the above three control factors that dominate the DA skill improvement, we also examine the top factor that
 475 affects SMAP L4 performance, i.e., vertical-coupling errors (Fig. 89). As expected, larger (absolute) bias in SSM-
 476 RZSM coupling in CLSM tends to be associated with degraded OL estimates of both SSM and RZSM (see Figs. 8a-
 477 b), although the analysis does not prove such a causal relationship. Similar to precipitation errors above, decreased OL
 478 skill (seen on the left-hand-side of the figures) provides an opportunity for increased DA skill improvement – which
 479 is clearly seen in Fig. 89. However, such increases are much larger for SSM than for RZSM.

480 For RZSM, SSM-RZSM coupling bias exerts both positive and negative effects on estimation accuracy. While such
 481 bias leads to an enhanced opportunity to improve upon a degraded OL, it should also hamper the ability of DA to

482 transfer SSM increments into the root-zone – particularly when, like here, the bias reflects the lack of vertical coupling
 483 in the model (Kumar et al., 2009). This means that some of the opportunity presented by the larger RZSM errors in
 484 OL is squandered by sub-optimal DA. As a result, the increase in RZSM DA skill improvement associated with biased
 485 SSM-RZSM coupling (Fig. 8e9d) is smaller than the analogous increase in SSM DA skill improvement (Fig. 8e9c).



486

487

488 **Figure 89:** As in Fig. 6-7 but for R_{OL} and ΔR as a function of SSM-RZSM coupling error indicated by the CP difference
489 ($\Delta CP = CP_{OL} - CP_{obs}$).

490

491 For the three strongest control factors that determine DA skill improvement ΔR , i.e., Tb ~~innovationerror~~, precipitation
492 error and microwave soil roughness, we further conducted paired one-way analysis of variance. Results indicates that
493 for each of the five binned groups separated by each of the above-mentioned three control factors, the inter-group
494 difference in ΔR caused by each control factor is significant ($p < 0.01$) for both SSM and RZSM. In addition, except for
495 the groups with lowest mean ΔR in Fig. 5a-6a and Fig. 7a8a, the averages of ΔR from all groups are significantly higher
496 than 0 ($p < 0.01$).

497 **4 Conclusions**

498 The SMAP L4 algorithm assimilates L-band Tb observations into the Catchment Land Surface Model to provide
499 surface and root-zone soil moisture estimates (i.e., SSM, RZSM) with global, 3-hourly coverage at 9-km resolution.

500 The performance of the L4 soil moisture estimates compared to a baseline model-only simulation (OL) is influenced
501 by multiple control factors associated with CLSM and the tau-omega RTM components of the L4 system. In this study,
502 we assess the performance of SMAP L4 DA system using two years of in-situ soil moisture profile observations at
503 2474 sites across mainland China. We apply a random forest (RF) regression to identify the dominant factors (from a
504 pre-defined list) that control the spatial distribution of the DA skill improvement (defined as the skill difference

505 between the L4 and OL estimates of SSM and RZSM as measured by their Spearman rank correlation with in-situ
506 measurements). Results show that L4 improves SSM prediction skill by 14% on average, with over 77% of the 2287
507 9-km EASE grid cells showing an increase in Spearman's rank correlation with in-situ observations. Similarly,
508 widespread, though smaller, improvements are observed in RZSM, with averaged *R* improvement of 7%.

509 Based on the RF regression analysis, the benefit of SMAP L4 DA for SSM is primarily determined by Tb innovation
510 ~~error~~ (measured by standard deviation of O-F Tb residuals), followed by microwave soil roughness and daily
511 precipitation error. These three factors are also the most prominent factors controlling SMAP DA improvement for
512 RZSM, albeit with the Tb innovation error being the least important of these three factors for RZSM DA skill
513 improvement.

514 Generally, the OL performance clearly decreases with increasing precipitation error, whereas for L4 performance
515 precipitation error is not identified as the most dominant control factor. This indicates that the L4 system is able to
516 correct for errors in precipitation forcing. In addition, our results demonstrate that SMAP DA contributes the most
517 benefit for cases where CLSM underestimates SSM-RZSM vertical coupling strength. However, due to the difference
518 in top-layer soil depth between the in-situ observations (10 cm) and the L4 analysis (5 cm), it is unclear whether or not
519 the observed SSM-RZSM coupling strength biases are real in an absolute sense – or simply reflect inconsistencies in
520 the depth of modelled versus observed SSM and RZSM time series. Nevertheless, it is worth stressing that, despite the
521 ambiguity about their absolute magnitude/sign, relative variations in apparent SSM-RZSM coupling biases explain a

522 significant amount of the observed spatial variation in L4 performance. Therefore, this finding clearly underpins the
523 importance of properly specifying SSM-RZSM coupling strength in CLSM as a way to improve the SMAP L4 product.

524 For SMAP L4 SSM skill, the next-most important factors (after SSM-RZSM coupling) are the precipitation error, the
525 Tb ~~innovation error~~ and microwave soil roughness (Fig. 445d). For L4 RZSM skill, the next-most important factors
526 (after SSM-RZSM coupling) are the precipitation error, the Tb ~~innovation~~ error and the LE error, with the latter two
527 factors of comparable importance (Fig. 445d). To enhance the L4 performance, additional focus should thus be placed
528 on improving the model's characterization of the microwave radiative transfer modeling (Tb ~~innovationerror~~), together
529 with the partitioning of the available energy into latent and sensible heat (LE error).

530 Some of our RF analysis results fall squarely within expectation; for instance, the OL skill is predominately determined
531 by precipitation error, which is in line with the previous studies using core validation site, sparse network sites and
532 other microwave soil moisture datasets (Reichle et al., 2017a, 2021; Dong et al., 2019a), and L4 skill improvement
533 (i.e., $R_{L4} - R_{OL}$) is mostly determined by Tb ~~innovationerror~~. On the other hand, there are also some more surprising
534 results. For instance, we found that SSM-RZSM coupling error and precipitation error have a comparable impact on
535 OL. For L4 skill, however, the impact of SSM-RZSM coupling error exceeds that of precipitation error. More
536 specifically, L4 DA contributes the most benefit for cases where CLSM underestimates SSM-RZSM vertical coupling
537 strength. This is the first quantification of the impact of different DA aspects (including background model structure
538 error and model input error) on DA performance. These findings could be used for L4 product development. In addition,

539 this study pinpoints that the L4 skill improvement is not heavily impacted by LAI magnitude, which gives confidence
540 for using the L4 product over densely vegetated areas.

541 **Data availability**

542 The SMAP L4 datasets are available from <https://nsidc.org/data/SPL4SMAU/versions/4>. Gauge-based precipitation
543 dataset CGDPA is from http://data.cma.cn/data/cdcdetail/dataCode/SEVP_CLI_CHN_PRE_DAY_GRID_0.25.html.

544 The availabilities of other datasets are stated in their corresponding subsections.

545 **Author contributions**

546 Jianxiu Qiu and Jianzhi Dong conceptualized the study. Jianxiu Qiu carried out the analysis and wrote the first draft
547 manuscript, Wade Crow refined the work, Jianzhi Dong, Rolf Reichle, and Gabrielle De Lannoy helped with the analysis.

548 All authors contributed to the analysis, interpretation of the results and writing.

549 **Competing interests**

550 The authors declare that they have no conflict of interest.

551 **Acknowledgments**

552 This work was supported by National Natural Science Foundation of China (Grant Nos. 41971031, 41501450). Rolf
553 Reichle was supported by the NASA SMAP mission. Gabrielle De Lannoy was supported by KU Leuven C1

554 (C14/16/045). The findings, conclusions and representations of fact in this publication are those of the authors and should
555 not be construed to represent any official USDA or U.S. Government determination or policy.

556 **References**

557 Baret, F., Weiss, M., Lacaze, R., Camacho, F., Makhmara, H., Pacholczyk, P., and Smets, B.: GEOV1: LAI, FAPAR
558 Essential Climate Variables and FCOVER global time series capitalizing over existing products. Part I: Principles of
559 development and production, *Remote Sens. Environ.*, 137, 299-309, doi:10.1016/j.rse.2013.02.030, 2013.

560
561 Bolten, J.D. and Crow, W.T.: Improved prediction of quasi-global vegetation conditions using remotely-sensed
562 surface soil moisture, *Geophys. Res. Lett.*, 39(19), doi:10.1029/2012GL053470, 2012.

563
564 Breiman, L.: Random forests, *Mach. Learn.*, 45(1), 5–32, doi:10.1023/A:1010933404324, 2001.

565
566 Chan, S., Njoku, E. G. and Colliander A.: SMAP L1C radiometer half-orbit 36 km EASE-Grid brightness temperatures,
567 version 3. NASA National Snow and Ice Data Center Distributed Active Archive Center, 10.5067/E51BSP6V3KP7,
568 2016.

569

570 Chen, F., Crow, W.T., Starks, P.J. and Moriasi, D.N.: Improving hydrologic predictions of a catchment model via
571 assimilation of surface soil moisture, *Adv. Water Resources.*, 34(4), 526-536, doi:10.1016/j.advwatres.2011.01.011,
572 2011.

573
574 Chen, F., Crow, W.T., Colliander, A., Cosh, M.H., Jackson, T.J., Bindlish, R., Reichle, R.H., Chan, S.K., Bosch, D.D.,
575 Starks, P.J., and Goodrich, D.C.: Application of triple collocation in ground-based validation of Soil Moisture
576 Active/Passive (SMAP) level 2 data products, *IEEE JSTARS.*, 99, 1-14, doi:10.1109/JSTARS.2016.2569998, 2016.

577
578 Crow, W.T. and Van Loon, E.: The impact of incorrect model error assumptions on the sequential assimilation of
579 remotely sensed surface soil moisture, *J. Hydrometeorol.*, 8(3), 421-431, doi:10.1175/jhm499.1, 2006.

580
581 [Dai, Y., Q. Xin, N. Wei, Y. Zhang, W. Shangguan, H. Yuan, S. Zhang, S. Liu, and X. Lu.: A global high-resolution](#)
582 [dataset of soil hydraulic and thermal properties for land surface modeling, *J. Adv. Model. Earth System*, 11\(9\), 2996-](#)
583 [3023, doi:10.1029/2019MS001784, 2019.](#)

584
585 De Lannoy, G. J. M., Reichle, R. H., and Pauwels, V. R. N.: Global calibration of the GEOS-5 L-band microwave
586 radiative transfer model over nonfrozen land using SMOS observations, *J. Hydrometeorol.*, 14(3), 765-785,
587 doi:10.1175/JHM-D-12-092.1, 2013.

588

589 De Lannoy, G. J. M., Reichle, R. H., and Vrugt, J. A.: Uncertainty quantification of GEOS-5 L-band radiative transfer
590 model parameters using Bayesian inference and SMOS observations, *Remote Sens. Environ.*, 148, 146–157,
591 doi:10.1016/j.rse.2014.03.030, 2014a.

592
593 [De Lannoy, G. J. M., Koster, R. D., Reichle, R. H., Mahanama, S. P. P., & Liu, Q.: An updated treatment of soil texture](#)
594 [and associated hydraulic properties in a global land modeling system. *J. Adv. Model. Earth System*, 6, 957–979. doi:](#)
595 [10.1002/2014MS000330, 2014b.](#)

596
597 Dong, J., Crow, W.T., Reichle, R., Liu, Q., Lei, F., and Cosh, M.: A global assessment of added value in the SMAP
598 Level 4 soil moisture product relative to its baseline land surface model, *Geophys. Res. Lett.*, 46, 6604-6613,
599 doi:10.1029/2019GL083398, 2019a.

600
601 Dong, J., Crow, W.T., Duan, Z., Wei, L., and Lu, Y.: A double instrumental variable method for geophysical product
602 error estimation, *Remote Sens. Environ.*, 225, 217-228, doi:10.1016/j.rse.2019.03.003, 2019b.

603
604 Dong, J., Crow, W.T., Tobin, J. K., Cosh, H. M., Bosch, D. D., Starks, J. P., Seyfried, M., and Collins, H. C.:
605 Comparison of microwave remote sensing and land surface modeling in surface soil moisture climatology estimation,
606 *Remote Sens. Environ.*, 242, 111756, doi :10.1016/j.rse.2020.111756, 2020.

607

608 Entekhabi, D., Njoku, E. G., O'Neill, P. E., Kellogg, K. H., Crow, W. T., and Edelstein, W. N.: The soil moisture active
609 passive (SMAP) mission, *P. IEEE.*, 98(5), 704–716, doi:10.1109/jproc.2010.2043918, 2010.

610
611 FAO/IIASA/ISRIC/ISSCAS/JRC (2012), Harmonized World Soil Database (version 1.2), Food and Agric. Organ.,
612 Rome. Available at: <http://webarchive.iiasa.ac.at/Research/LUC/External-World-soil-database/HTML>.

613
614 Gupta, H. V., Kling, H., Yilmaz, K. K., and Martinez, G. F.: Decomposition of the mean squared error and NSE
615 performance criteria: Implications for improving hydrological modelling, *J. Hydrometeorol.*, 377(1-2), 80-91,
616 doi:10.1016/j.jhydrol.2009.08.003, 2009.

617
618 Han, S., Shi, C. X., Jiang, L. P., Zhang, T., Liang, X., Jiang, Z. W., Xu, B., Li, X. F., Zhu, Z., Lin, H. J.: The simulation
619 and evaluation of soil moisture based on CLDAS, *J. Applied Meteorol. Sci.*, 28(3), 369-378, doi:10.11898/1001-
620 7313.20170310, 2017.

621
622 [Hillel, D., 1998. Environmental soil physics: Fundamentals, applications, and environmental considerations. Academic](#)
623 [press.](#)

624
625 Jung, M., Koirala, S., Weber, U., Ichii, K., Gans, F., Camps-Valls, G., and Reichstein, M.: The FLUXCOM ensemble
626 of global land-atmosphere energy fluxes, *Sci. Data.*, 6(1), 1-14, doi:10.1038/s41597-019-0076-8, 2019.

627

628 Kumar, S.V., Reichle, R.H., Koster, R.D., Crow, W.T., and Peters-Lidard, C.D.: Role of subsurface physics in the
629 assimilation of surface soil moisture observations, *J. Hydrometeorol.*, 10, 1534-1547, doi:10.1175/2009JHM1134.1,
630 2009.

631

632 Lucchesi, R.: File specification for GEOS-5 FP, NASA GMAO Office Note 4 (version 1.0), 63 pp. Available at
633 <https://ntrs.nasa.gov>, 2013.

634

635 Mahanama, S. P., Koster R. D., Walker G. K., Takacs L. L., Reichle R. H., De Lannoy G., Liu Q., Zhao B., and Suarez
636 M. J.: Land boundary conditions for the Goddard Earth Observing System model version 5 (GEOS-5) climate modeling
637 system—Recent updates and data file descriptions. NASA/TM-2015-104606, Vol. 39, 55 pp. NASA Goddard Space
638 Flight Center, Greenbelt, MD. Available at <https://ntrs.nasa.gov/search.jsp?R=20160002967>, 2015.

639

640 McColl, K., Vogelzang, J., Konings, A.G., Entekhabi, D., Piles, M., and Stoffelen, A.: Extended triple collocation:
641 Estimating errors and correlation coefficients with respect to an unknown target, *Geophys. Res. Lett.*, 41(17), 6229-
642 6236, doi:10.1002/2014gl061322, 2014.

643

644 Piepmeier, J. R., Focardi, P., Horgan, K. A., Knuble, J., Ehsan, N., Lucey, J., Brambora, C., Brown, P. R., Hoffman,
645 P. J., French, R. T., Mikhaylov, R. L., Kwack, E. Y., Slimko, E. M., Dawson, D. E., Hudson, D., Peng, J., Mohammed,

646 P. N., de Amici, G., Freedman, A. P., Medeiros, J., Sacks, F., Estep, R., Spencer, M. W., Chen, C. W., Wheeler, K. B.,
647 Edelstein, W. N., O'Neill, P. E., and Njoku, E. G.: SMAP L-band microwave radiometer: Instrument design and first
648 year on orbit, *IEEE T. Geosci. Remote.*, 55(4), 1954–1966, doi:10.1109/TGRS.2016.2631978, 2017.

649
650 Liu, Q., Reichle, R., Bindlish, R., Cosh, M.H., Crow, W.T., de Jeu, R., de Lannoy, G., Huffman, G.J. and Jackson,
651 T.J.: The contributions of precipitation and soil moisture observations to the skill of soil moisture estimates in a land
652 data assimilation system, *J. Hydrometeorol.*, 12(5), 750-765, doi:10.1175/JHM-D-10-05000.1, 2011.

653
654 Reichle, R.H., Crow, W.T., Koster, R. D., Sharif, H. and Mahanama, S.: Contribution of soil moisture retrievals to
655 land data assimilation products, *Geophys. Res. Lett.*, 35(1), doi:10.1029/2007GL031986, 2008.

656
657 Reichle, R. H., de Lannoy, G. J. M., Liu, Q., Ardizzone, J. V., Colliander, A., Conaty, A., Crow, W., Jackson, T. J.,
658 Jones, L. A., Kimball, J. S., Koster, R. D., Mahanama, S. P., Smith, E. B., Berg, A., Bircher, S., Bosch, D., Caldwell,
659 T. G., Cosh, M., González-Zamora, Á., Holifield Collins, C. D., Jensen, K. H., Livingston, S., Lopez-Baeza, E.,
660 Martínez-Fernández, J., McNairn, H., Moghaddam, M., Pacheco, A., Pellarin, T., Prueger, J., Rowlandson, T., Seyfried,
661 M., Starks, P., Su, Z., Thibeault, M., van der Velde, R., Walker, J., Wu, X., and Zeng, Y.: Assessment of the SMAP
662 Level-4 surface and root-zone soil moisture product using in situ measurements, *J. Hydrometeorol.*, 18(10), 2621–
663 2645, doi:10.1175/JHM-D-17-0063.1, 2017a.

664

665 Reichle, R. H., de Lannoy, G. J. M., Liu, Q., Koster, R. D., Kimball, J. S., Crow, W. T., Ardizzone, J. V., Chakraborty,
666 P., Collins, D. W., Conaty, A. L., Giroto, M., Jones, L. A., Kolassa, J., Lievens, H., Lucchesi, R. A., and Smith, E. B.:
667 Global assessment of the SMAP Level-4 surface and root-zone soil moisture product using assimilation diagnostics, *J.*
668 *Hydrometeorol.*, 18(12), 3217–3237, doi:10.1175/jhm-d-17-0130.1, 2017b.

669

670 Reichle, R. H., de Lannoy, G., Koster, R. D., Crow, W. T., Kimball, J. S., and Liu, Q.: SMAP L4 Global 9 km EASE-
671 grid surface and root zone soil moisture land model constants, Version 4, NASA National Snow and Ice Data Center
672 DAAC, <https://doi.org/10.5067/KGLC3UH4TMAQ>, 2018a.

673

674 Reichle, R. H., de Lannoy, G., Koster, R. D., Crow, W. T., Kimball, J. S., & Liu, Q.: SMAP L4 global 3-hourly 9 km
675 EASE-grid surface and root zone soil moisture analysis update data, version 4, NASA National Snow and Ice Data
676 Center DAAC, <https://doi.org/10.5067/60HB8VIP2T8W>, 2018b.

677

678 Reichle, R. H., de Lannoy, G., Koster, R. D., Crow, W. T., Kimball, J. S., & Liu, Q.: SMAP L4 global 3-hourly 9 km
679 EASE-grid surface and root zone soil moisture geophysical data, version 4, NASA National Snow and Ice Data Center
680 DAAC, <https://doi.org/10.5067/KPJNN2GI1DQR>, 2018c.

681

682 Reichle, R. H., Liu, Q., Koster, R. D., Crow, W. T., De Lannoy, G. J., Kimball, J. S., and Kolassa, J.: Version 4 of the
683 SMAP Level-4 soil moisture algorithm and data product, *J. Adv. Model Earth Sy.*, 11(10), 3106-3130,
684 doi:10.1029/2019MS001729, 2019.

685
686 Reichle, R. H., and Coauthors.: The contributions of gauge-based precipitation and SMAP brightness temperature
687 observations to the skill of the SMAP Level-4 soil moisture product, *J. Hydrometeorol.*, [accepted in press](#),
688 doi:10.1175/JHM-D-20-0217.1, [2021](#).

689
690 Seneviratne, S. I., Corti, T., Davin, E. L., Hirschi, M., Jaeger, E. B., and Lehner, I.: Investigating soil moisture–climate
691 interactions in a changing climate: A review, *Earth-Sci. Rev.*, 99, 125–161, doi:10.1016/j.earscirev.2010.02.004, 2010.

692
693 Seneviratne, S. I., Wilhelm, M., Stanelle, T., Hurk, B., Hagemann, S., and Berg, A.: Impact of soil moisture–climate
694 feedbacks on CMIP5 projections: First results from the GLACECMIP5 experiment, *Geophys. Res. Lett.*, 40(19), 5212-
695 5217, doi:10.1002/grl.50956, 2013.

696
697 Shen, Y., Xiong, A., Wang, Y., and Xie, P.: Performance of high-resolution satellite precipitation products over China,
698 *J. Geophys. Res-Atmos.*, 115(D2), doi:10.1029/2009JD012097, 2010.

699

700 Shen, Y. and Xiong, A.: Validation and comparison of a new gauge-based precipitation analysis over mainland China,
701 Int. J. Climatol., 36(1), 252-265, doi:10.1002/JOC.4341, 2015.

702

703 Verger, A., Baret, F., and Weiss, M.: Performances of neural networks for deriving LAI estimates from existing
704 CYCLOPES and MODIS products, Remote Sens. Environ., 112, 2789-2803, doi:10.1016/j.rse.2008.01.006, 2008.

705

706 Xie, P., Yatagai, A., Chen, M., Hayasaka, T., Fukushima, Y., Liu, C., and Yang, S.: A gauge-based analysis of daily
707 precipitation over East Asia, J. Hydrometeorol., 8, 607-626, doi:10.1175/JHM583.1, 2007.

708

709 Xie, P., Joyce, R., Wu, S., Yoo, S.-H., Yarosh, Y., Sun, F., Lin, R.: NOAA CDR Program: NOAA Climate Data
710 Record (CDR) of CPC Morphing Technique (CMORPH) High Resolution Global Precipitation Estimates, Version 1.
711 NOAA National Centers for Environmental Information, 2019.